Electronic Materials Letters, Vol. 5, No. 3 (2009), pp. 99-103
DOI: 10.3365/eml.2009.09.099

Microstructure Evolution of Al-1% Si Bonding Wire for Microelectronic Reliability

Hyung-Giun Kim,[1] Dae–Hyung Cho,[2] Eun-Kyun Jeong,[2] Won–Yong Kim,[3] and Sung–Hwan Lim[1,*]

[1]Department of Advanced Materials Science and Engineering, Kangwon National University, Chuncheon-si, Gangwon 200-701, Korea
[2]R&D Department, Heraeus Oriental HiTec, Incheon 587-122, Korea
[3]Advanced Materials R&D Center, Korea Institute of Industrial Technology, Incheon 406-130, Korea

In order to determine the reliability of Al-1% Si bonding wires, the microstructure of an annealed wire, including grain morphology and secondary phases, was investigated by conventional transmission electron microscopy (TEM) and high-resolution electron microscopy (HREM). The grains are extremely long and thin parallel to the drawn direction, and the average grain size is about 600 nm to 700 nm. Nano-sized thin plate-like Si crystals of about 10 nm length and a few monolayers thickness were observed, and their crystallography and morphology are discussed in this paper.

Keywords: Al-Si bonding wires, Si crystals, Microstructure, TEM, HREM

1. INTRODUCTION

Al-Si bonding wires are used to interconnect chips in microelectronic devices such as RF power transistors. Figure 1 is a typical image of Al-Si bonding wires used in a chip, which may contain many RF power transistors. Generally, in order to ensure that uniform, high-quality Al-Si bonding wires can be obtained, about 1% Si is added to high-purity aluminum to strengthen it.[1] Previous research on Al-Si bulk materials[2] has shown that the Si-phase precipitates grow to about 20 nm and that they have a round shape during the annealing process. However, further growth results in plate-like structure Si-phase precipitates in the Al matrix: $\{111\}_{Si}$, which are known to be formed parallel to $\{111\}_{Al}$, $\{100\}_{Al}$, and $\{110\}_{Al}$.[3,4] Nakagawa *et al.*[5] have investigated the Al-1.2% Si bulk alloy in the early stage of annealing, and concluded that the Si clusters, after rapid cooling, act as nuclei for the Si-phase precipitates. Moreover, since the drawing and annealing processes in producing the Al-Si bonding wires yield a textured structure at the given temperatures, microstructural properties seem to be sensitive to and influenced by thermomechanical processes. Liu *et al.*[6] have reported that the strength of Al-1.2% Si bonding wire is greater than the bulk material whose strength results from nanoparticle (Si) hardening and texture strengthening. Consequently, the microstructural properties of bonding wire effected by heating the area adjacent to the formed ball during the bonding process can be expected to be much different from those of bulk materials. Therefore, microstructural properties can be directly correlated to bonding reliability, one of the important characteristics of bonding wires.[7] Although some metallurgical and mechanical properties of Al-Si bonding wires have been reported,[8,9] there have been few detailed studies on their microstructural characteristics.[6,10] Transmission electron microscopy (TEM) is a valuable technique that enables microstructural characteristics to

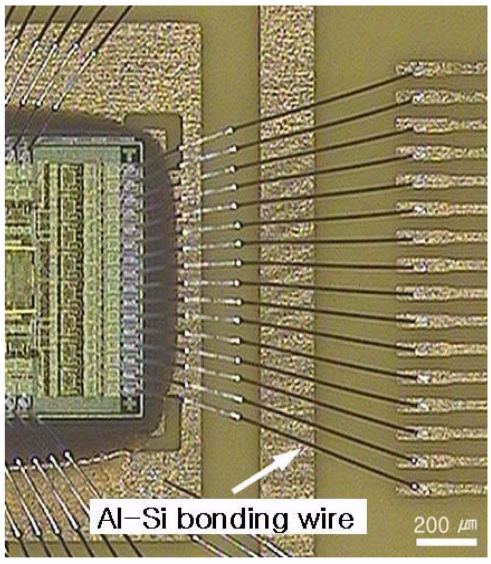

Fig. 1. Optical micrograph of Al-Si bonding wires in a device containing many RF power transistors. The wire diameter is about 30 μm.

*Corresponding author: shlim@kangwon.ac.kr

be ascertained in real space.[11-13] The purpose of the present study was to investigate the microstructural characteristics, including the grain morphology and precipitates, of annealed Al-1% Si bonding wires by means of conventional TEM, high-resolution electron microscopy (HREM), and image processing techniques.

2. EXPERIMENTAL PROCEDURE

Al-1% Si ingots were cast by melting, in air, 99.99% Al and 99.99%Si in a high-purity alumina crucible. The ingots obtained were then homogenized by annealing, peeled mechanically, hot forged, and cold drawn with intermediate annealing to produce wire of 32 μm diameter. The Al-1% Si bonding wires subsequently were heat treated at 553 K for 2 s, then rapidly cooled to 273 K. Specimens for TEM observation were prepared by two different methods, one parallel to the drawn direction (D.D.), and the other perpendicular to the drawn direction (T.D.). The specimen preparation method for observation along the D.D. is shown in Figs. 2(a) and (b). About 200 Al-Si bonding wires and epoxy resin were put into a brass tube of 3 mmϕ outer diameter and 2 mmϕ inner diameter. Given that there were many pores between the bonding wires, the epoxy resin was hardened for several hours to reduce these pores. A disk of about 0.5 mm thickness was cut from the tube, mechanically polished to about 30 μm in thickness, and then dimpled to 20 μm in the center. Both sides of the disk were reinforced with grids of 3 mmϕ diameter with a 1 mmϕ hole, and then the disk was thinned by Ar ion milling until it became electron-transparent. Specimen for the observation of the T.D. cross-section was prepared as shown in Figs. 2(c) and (d). About thirty wires were arranged on the center of a grid and adhered with epoxy resin. The grid was reinforced with another grid and thinned by Ar ion milling. TEM observations of the microstructural characteristics, including the grain morphology were carried out under a JEOL-2000EX microscope at 200 kV. The microstructural characteristics of the precipitates were investigated under a JEM-ARM 1300S electron microscope at 1250 kV.

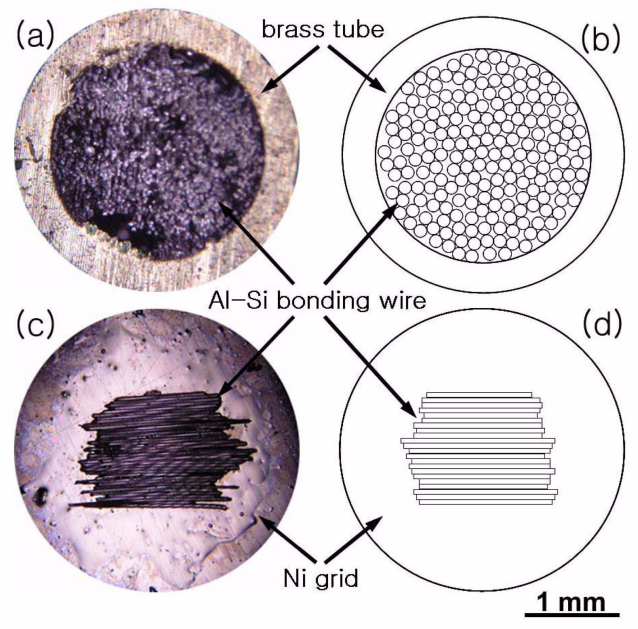

Fig. 2. Illustration of TEM specimen preparation: (a) and (b), Al-Si bonding wires are inserted into brass tubes, and a disk including Al-Si bonding wires is reinforced with a grid for observation of D.D. cross-section; (c) and (d), Al-Si bonding wires are arranged on grid and adhered with epoxy resin for TEM observation of T.D. cross-section.

3. RESULTS AND DISCUSSION

Figure 3(a) shows a bright-field image of the D.D. cross-sectional view of a bonding wire thinned by ion milling. The grains of the wire are very fine. The average size of the grains is approximately 600 nm to 700 nm. The large black rectangle of Fig. 3(a) encompasses an enlarged image of the dislocation loop that is thought to be the result of heavy deformation and the secondary phases, indicated by arrows, within the small black rectangle. The secondary phases are fine and uniform, and they interact with dislocations, result-

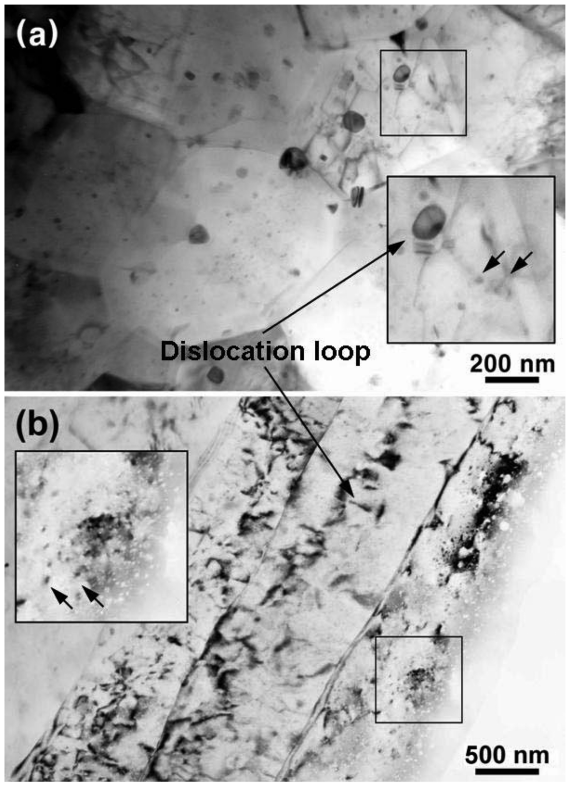

Fig. 3. (a) Bright-field image of D.D. cross-sectional view of wire thinned by ion milling, (b) Bright-field image of center of wire cross-section observed perpendicular to drawn direction (T.D. cross-sectional view).

ing effectively in enhanced wire strength. Figure 3(b) shows a bright-field image of the center of the T.D. cross-sectional view. The grains are extremely long and thin parallel to the drawn direction, and the average grain size perpendicular to the drawn direction is about 600 nm to 700 nm. This grain size corresponds to that shown in Fig. 3(a). As is evident in the image, there was no change in grain size over the entire area. The large black rectangle of Fig. 3(b) encompasses an enlarged image of the dark-contrast secondary phases, of less than 15 nm size, indicated by the arrows within the small black rectangle. Since the long axis of the fine grains in Fig. 3(b) is in the <111> direction in the diffraction patterns (not shown), it is clear that a <111> texture is formed parallel to the drawn direction by the drawing. The deviation from the <111> direction of some adjacent grains is only a few degrees. The annealed structure is of fine texture and grains of <111> orientation. The crystal structure of the secondary phases could not be identified unambiguously from the conventional TEM observations; to obtain further structural information, HREM observations, therefore, were carried out. Figure 4(a) shows an HREM image, taken with the incident beam along the $[011]_{Al}$ zone axis, of the same specimen shown in Fig. 3(a). The moiré fringe region (A) as well as a small area with white contrast (B) is clearly observed. Figure 4(b) shows an image of the moiré fringe region formed by interference between Al and precipitate reflections, which region is encompassed by the white rectangle (A) shown enlarged in Fig. 4(a). These moiré fringes are nearly parallel to the $(11\bar{1})$ plane of the Al matrix. The fringe spacing measured on this image is about 0.91 nm. Figure 4(c) shows an enlarged image of the plate-like strain contrast features, encompassed by the white rectangle (B) in Fig. 4(a). This contrast is due to the local strain between the Al matrix and the precipitate in the annealed sample. The orientation of the plate-like small area of strain contrast to the matrix is parallel to $\{111\}_{Al}$; the atomic arrangement of the interface between the small area of white contrast and the matrix closely corresponds to the arrangement of the matrix. Therefore, the plate-like small area of white contrast and the Al matrix are coherent. The distance between two neighboring atoms in the small area of white contrast is shorter than that for $\{111\}_{Al}$, and a distorted region exists in the interface between the small area of white contrast and the matrix. A different set of moiré fringes was observed in other secondary phases in the same specimen, as shown in Fig. 5(a). The fringes, again, are nearly parallel to the $(11\bar{1})$ plane, with a fringe spacing of 0.92 nm. Figure 5(b) shows a Fourier-filtered image of Fig. 5(a) using all of the fundamental reflections. It is well known that when an incident electron beam passing through a specimen encounters an interface between two crystals of different lattice constants, it can give rise to moiré fringes in a TEM image.[12] If both the crystals of the

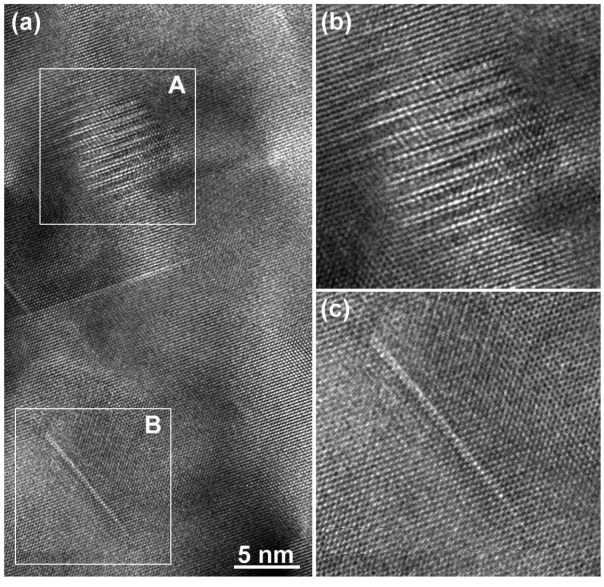

Fig. 4. (a) HREM image of specimen annealed at 553 K after quenching to 273 K. A small area with white contrast (A) and a moiré fringe region (B) can be seen, (b) Enlarged image of moiré fringe region formed by interference between Al- and Si-phase precipitate reflections, corresponding to white rectangular region A in Fig. 5(a), (c) Enlarged image of plate-like strain contrast features corresponding to region encompassed by white rectangle B in Fig. 5(a).

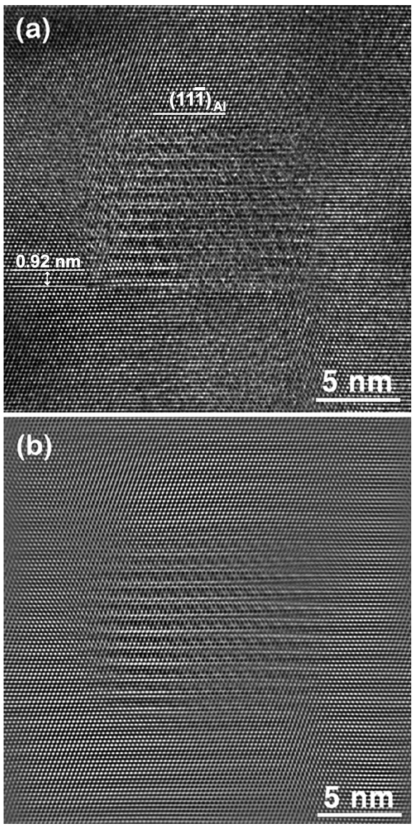

Fig. 5. (a) HREM image of Si-phase precipitate taken from annealed specimen. The moiré fringes are almost parallel to the $(11\bar{1})_{Al}$ plane, (b) Fourier-filtered image of HREM image in Fig. 5(a).

Al matrix and those of the secondary phase have parallel reflecting planes with different lattice constants, parallel moiré fringes result. The spacing for parallel moiré fringes, D, can be calculated from the following equation: $D = d_S \cdot d_{Al} / (d_S - d_{Al})$, where d_S is the interplanar spacing of the secondary phase and d_{Al} is the interplanar spacing of the Al matrix. If possible lattice contractions in the secondary phases due to surface stress are ignored it is reasonable to assume that the interplanar spacing of $(111)_{Al}$ of the d_{Al} is equal to that of pure Al, owing to the low solubility for Si. Using this value (0.233 nm) as a reference, the interplanar spacing of the secondary phase calculated from Fig. 5(a) equals 0.312 nm. This is consistent with the interplanar spacing of $\{111\}_{Si}$. Thus, it is concluded that the moiré fringes arise due to a lattice mismatch between the Al matrix and Si crystals. Further information on the secondary phase was gleaned from the diffractogram shown in Fig. 6, which was obtained by a digital Fourier analysis of Fig. 5(a). Only weak streaks parallel to $(111)_{Al}$ are seen with the Al matrix reflections in Fig. 6. This might be caused by lattice distortion of the Al matrix in the <111> direction as well as the thin plate-like morphology of the Si crystal. Figure 6 also shows that the weak extra spots with $\{111\}_{Si}$ are observed along the vector from the 000 spot to the diffraction spots on $\{111\}_{Al}$. This indicates that the moiré regions are parallel to the moiré pattern from the $\{111\}_{Si}$ and $\{111\}_{Al}$ planes. Therefore, it can be concluded that Si crystals of about 10 nm length and a few monolayers in thickness are formed in the thin plate-like Si structure on the $(111)_{Al}$ plane in both the small area with white contrast and in the moiré regions. When the Si phase precipitates are coherent with the Al matrix, the atomic size difference has a large influence on the morphology of the precipitates. However, when the Si-phase precipitates and the Al matrix are incoherent, the precipitates are influenced by the interface energy and tend to have a round-shaped morphology.[14] From the experimental results, we observed areas where the small areas with white contrast and $\{111\}_{Al}$ are coherent with each other at an annealing time of 2 sec. The difference of the atomic radii between the Al matrix and the Si crystals is about 4.2%. This is a very small difference compared to the values for the Al-Cu bulk alloys,[15] which form disc-shaped GP-zones with the coherency in the matrix. The precipitate that forms the surrounding distortion in the matrix forms along the direction parallel to the smallest elastic anisotropic constant of the matrix with the largest direction of distortion.[16] The plate-like Si-phase precipitates that are formed during the annealing stage become coherent in Al-1% Si bonding wires, and the $\{111\}_{Al}$ is one of the preferred crystallographic planes for reducing the elastic anisotropic constant in the matrix, which in turn leads to a reduction in the anisotropic distortion energy.

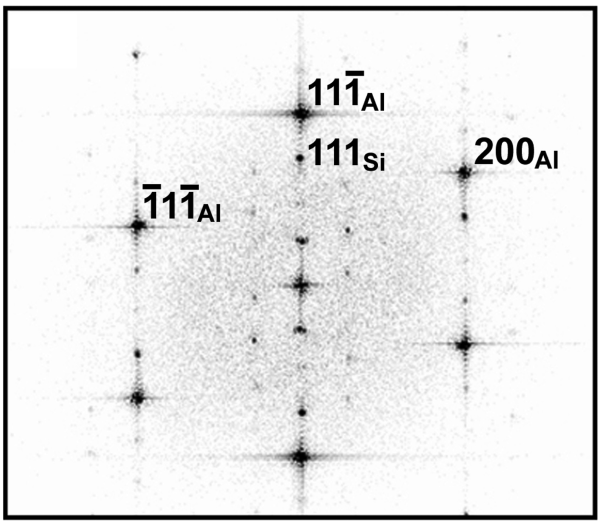

Fig. 6. Diffractogram taken from HREM image in Fig. 5(a).

4. CONCLUSIONS

Key components of the reliability of Al-Si bonding wires used in microelectronic devices, the crystallography and morphology of nano-sized secondary phases were investigated in a specimen annealed at 553 K for 2 s and observed under conventional TEM as well as HREM. The grains are extremely long and thin parallel to the drawn direction ; the average grain size perpendicular to the drawn direction is about 600 nm to 700 nm. Plate-like Si crystals of about 10 nm length and a few monolayers in thickness were observed in the $(111)_{Al}$ plane. The influence of Si crystals of diamond structure on the mechanical properties of bonding wires and their possible growth mechanisms under the annealing process will be addressed in subsequent papers.

ACKNOWLEDGMENTS

This work was supported by a Korea Research Foundation grant from the Korean Government (MOEHRD) (KRF-202-2004-D00433). This study was also supported by a Research Grant from Kangwon National University. The use of the electron microscope at the Korea Basic Science Institute is also greatly appreciated.

REFERENCES

1. H. S. Rosenbaum and D. Turnbull, *Acta Metall.* **7**, 664 (1983).
2. M. Nemoto and S. Koda, *J. Jpn. Inst. Met.* **29**, 399 (1965).
3. A. Saulnier, *Sci. Rev. Met.* **58**, 615(1961).
4. K. V. Ravl and E. Philofsky, Metall. Trans. **2**, 1089 (1971).
5. K. Nakagawa, T. Kanadani, L. Anthony, and H. Hashimoto, *Mater. Trans*. **46**, 779 (2005).
6. Y. Liu and W. K. Jones, *J. Elec. Mat*. **33**, 929 (2004).

7. G. G. Harman, *Wire Bonding in Microelectronics*, McGraw-Hill, New York (1997).
8. W. Qin, R. Doyle, T. Scharr, M. Shah, M. Kottke, G. Chen, and D. Theodore, *Microelec. Eng*. **75**, 111 (2004).
9. D. G. Davies and P. Douglas, *Metallurgy, Fabrication and Use of Al-1% Si Bonding Wire*, p. 1, American Fine Wire Corp (1991).
10. S. Remminger, N. Seliger, and G. Wachutka, *Microelec. Reliability* **40**, 1521 (2000).
11. D. Shindo and K. Hiraga, *High-Resolution Electron Microscopy for Materials Science*, Springer-Verlag, Tokyo (1998).
12. P. B. Hirsch, A. Howie, R. B. Nicholson, D. W. Pashley, and M. J. Whelan, *Electron Microscopy of Thin Crystals*, Butterworths, London (1965).
13. J. R. Yoon, D. J. Choi, K. –H. Lee, J. Y. Lee, and Y. –H. Kim, *Electron. Mater. Lett.* **4**, 167 (2008).
13. D. A. Porter and K. E. Easterling, *Phase Transformations in Metals and Alloys*, Van Nostrand Reinhold Co., New York (1981).
14. R. B. Nicholson and J. Nutting, *Philos. Mag*. **3**, 531 (1958).
15. F. J. Humphreys and M. Hatherly, *Recrystallization and Related Annealing Phenomena*, Pergamon (1995).